

# An A-D-A Type Small-Molecule Electron Acceptor with End-Extended Conjugation for High Performance Organic Solar Cells

Huanran Feng,<sup>†,||</sup> Nailiang Qiu,<sup>†,||</sup> Xian Wang,<sup>‡,||</sup> Yunchuang Wang,<sup>†</sup> Bin Kan,<sup>†</sup> Xiangjian Wan,<sup>†</sup> Mingtao Zhang,<sup>†</sup> Andong Xia,<sup>‡,||</sup> Chenxi Li,<sup>†</sup> Feng Liu,<sup>\*,§</sup> Hongtao Zhang,<sup>\*,†</sup> and Yongsheng Chen<sup>\*,†,||</sup>

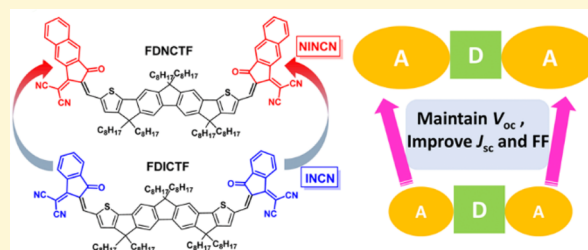
<sup>†</sup>State Key Laboratory of Elemento-Organic Chemistry, Centre of Nanoscale Science and Technology and Key Laboratory of Functional Polymer Materials, College of Chemistry, Nankai University, Tianjin 300071, China

<sup>‡</sup>Beijing National Laboratory for Molecular Sciences (BNLMS), Key Laboratory of Photochemistry, Institute of Chemistry, Chinese Academy of Sciences, Beijing 100190, China

<sup>§</sup>Department of Physics and Astronomy, Shanghai Jiaotong University, Shanghai 200240, China

## S Supporting Information

**ABSTRACT:** A new non-fullerene small molecule with an acceptor-donor-acceptor (A-D-A) structure, FDNCTF, incorporating fluorenedicyclopentathiophene as core and naphthyl-fused indanone as end groups, was designed and synthesized. Compared with the previous molecule FDICTF with the phenyl-fused indanone as the end groups, the extended  $\pi$ -conjugation at the end group has only little impact on its molecular orbital energy levels, and thus, the open-circuit voltage ( $V_{oc}$ ) of its solar cell devices has been kept high. However, its light absorption and mobility, together with the short-current density ( $J_{sc}$ ) and the fill factor (FF), of its devices have been all improved simultaneously. Through morphology, transient absorption, and theoretical studies, it is believed that these favorable changes are caused by (1) the appropriately enhanced molecular interaction between donor/acceptor which makes the charge separation at the interface more efficient, and (2) enhanced light absorption and more ordered packing at solid state, all due to the extended end-group conjugation of this molecule. With these, the solar cells with FDNCTF as the acceptor and a wide band gap polymer PBDB-T as the donor demonstrated a high power conversion efficiency (PCE) of 11.2% with an enhanced  $J_{sc}$  and a maintained high  $V_{oc}$ , and significantly improved FF of 72.7% compared with that of the devices of FDICTF with the phenyl-fused indanone as the end groups. These results indicate that the unexplored conjugation size of the end group plays a critical role for the performance of their solar cell devices.



## INTRODUCTION

Bulk heterojunction (BHJ) organic solar cells (OSCs) have attracted extensive attention due to their potentials in developing low cost, flexible, large-scale, and semitransparent solar panels.<sup>1–5</sup> Recently, benefiting from the rapid development of non-fullerene (NF) small-molecule acceptors due to their better absorption and tunable band structures, the overall performance of OSCs has improved significantly to 13%.<sup>6</sup> On the basis of the equation of  $PCE = J_{sc} \times V_{oc} \times FF/P_{in}$ , it is best to improve open-circuit voltage ( $V_{oc}$ ), short-circuit current ( $J_{sc}$ ), and fill factor (FF) simultaneously when further higher power conversion efficiency (PCE) is desired. Different with their inorganic counterparts, the charge separation of exciton in organic solar cells is mainly limited by its shorter effective diffusion length.<sup>7–9</sup> Both theoretical and experimental results have indicated that the charge separation efficiency is expected to be potentially improved by appropriately increasing the donor (D)/acceptor (A) intermolecular interaction.<sup>10–14</sup> On the other hand,  $V_{oc}$ ,  $J_{sc}$ , and FF are often tangled together as both molecular properties (i.e., conjugation length, band structure, etc.) and film morphology (the domain size and

interpenetrating network) in many cases may have an opposite impact on these factors. For example, while it is intrinsic to lower the lowest unoccupied molecular orbital (LUMO) level of the acceptor for higher  $J_{sc}$ , the corresponding  $V_{oc}$  could decrease accordingly.<sup>15,16</sup> Also, while the increased conjugation size of molecules may improve optical absorption, over extended size of the backbone and high degree of coplanarity tend to make the molecules over aggregated, thus leading to poor morphology with a large phase separation often for poor FF.<sup>17</sup> Therefore, a dedicated balance of molecule design is highly required to achieve not only high optical absorption and suitable energy level but also optimized film morphology.

In the past few years, to maximize PCE, much work has been focused on the design of various small molecules containing different electron-deficient groups, such as perylene diimide (PDI), naphthalene diimide (NDI), diketopyrrolopyrrole (DPP), tetraazabenzodifluoroanthene diimide, rhodanine, and

Received: July 6, 2017

Revised: August 29, 2017

Published: August 29, 2017

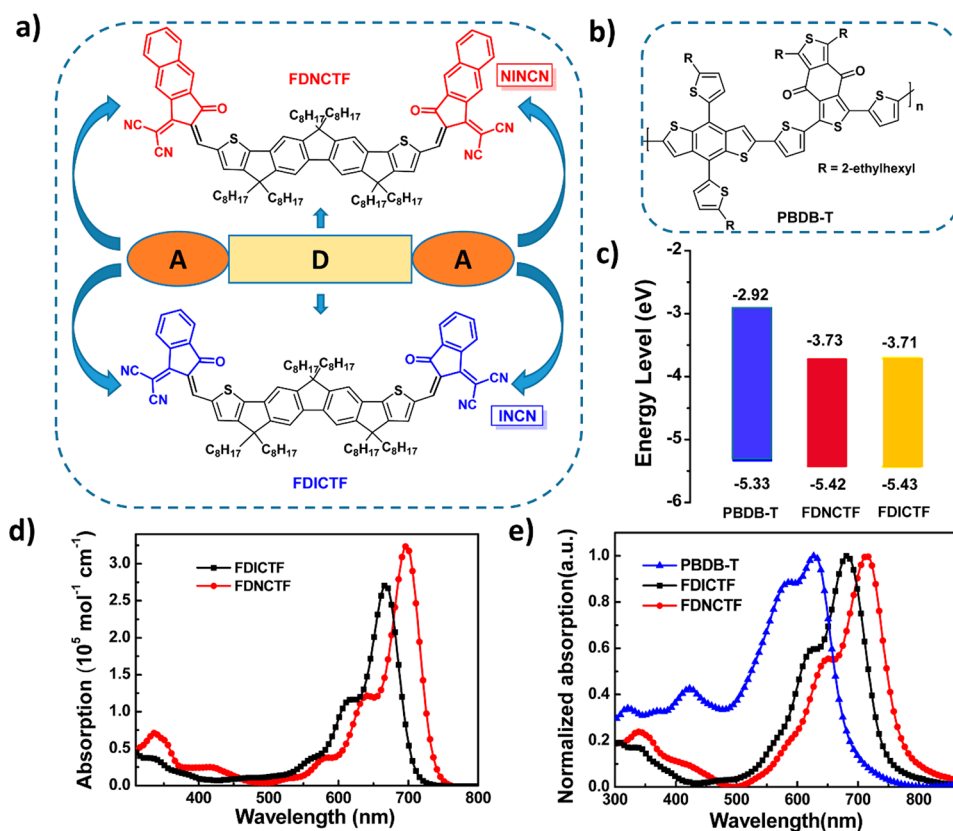


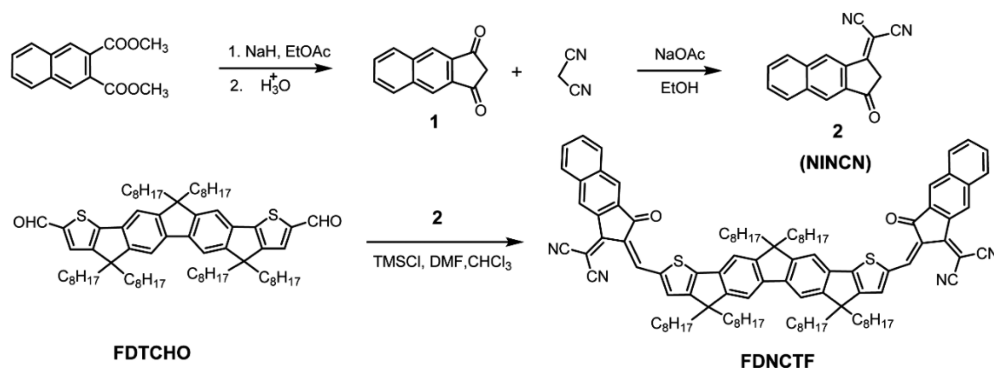
**Figure 1.** Chemical structures of (a) FDICTF and FDNCTF and (b) PBDB-T donor. (c) Estimated energy levels of FDICTF, FDNCTF, and PBDB-T from electrochemical cyclic voltammetry. (d) UV-vis absorption spectra of FDICTF and FDNCTF in chloroform solution. (e) UV-vis absorption spectra of PBDB-T, FDICTF, and FDNCTF in neat film.

2-(3-oxo-2,3-dihydro-1*H*-inden-1-ylidene)malononitrile (INCN) as NF acceptors.<sup>18–22</sup> Interestingly, it should be noted that, currently, the most successful NF molecules all have the same acceptor-donor-acceptor (A-D-A) molecular architecture which has been proved to be very successful for many donor molecules in the last 10 years.<sup>6,22,23</sup> Some of these high performance A-D-A type NF molecules include ITIC (3,9-bis(2-methylene-(3-(1,1-dicyanomethylene)-indanone)-5,5,11,11-tetrakis(4-hexylphenyl)-dithieno[2,3-*d*:2',3'-*d'*]-*s*-indaceno[1,2-*b*:5,6-*b'*]-dithiophene),<sup>23</sup> INIC (3,9-bis(2-methylene-(3-(1,1-dicyanomethylene)-indanone)-6,6,12,12-tetrakis(4-hexylphenyl)-indacenobis(dithieno[3,2-*b*:2',3'-*d*]thiophene),<sup>24</sup> and IDTBR (5*Z*,5'*Z*)-5,5'-{[5,5,11,11-tetrakis(*n*-octyl)-dithieno[2,3-*d*:2',3'-*d'*]-*s*-indaceno[1,2-*b*:5,6-*b'*]dithiophene=2,8-diyl}bis[2,1,3-benzothiadiazole-7,4-diyl(*Z*)methylidene]}-bis(3-ethyl-2-thioxo-1,3-thiazolidin-4-one)),<sup>22</sup> and PCEs over 13% based on these A-D-A small-molecule acceptors have been achieved.<sup>6</sup> The reasons behind the much success of the A-D-A architecture might be very complicated and are yet to be fully understood. However, some arguments we have are (1) the spatial distribution of the electron density of frontier molecular orbitals (HOMO and LUMO) of this type of molecules might favor the important charge separation at the interface of the donor and acceptor; (2) the easily tuned absorptions and energy levels of these A-D-A molecules; and (3) the optimal (not too high not too low) aggregation of the molecules due to their structure at solid state. It should be noted that most of these successful NF acceptors comprise aromatic fused rings with extended conjugation as the donor core and an electron-deficient conjugation unit as the end groups, which would

prompt intermolecular  $\pi$ - $\pi$  overlaps and enhance intermolecular charge transport. The large central  $\pi$ -conjugated unit would result in better absorption; thus, higher  $J_{sc}$  could be achieved.<sup>24–27</sup> However, compared with many studies on the central core unit for these A-D-A small-molecule acceptors,<sup>24,28–30</sup> no larger conjugation end unit (almost all are based on INCN end unit) has been studied to understand the influence of extended end groups on the properties of these molecules.<sup>24,31</sup> This is contrary to the intensive studies carried out for the small-molecule donors, where tuning the end groups would improve the material performance significantly.<sup>32–34</sup> On the other hand, extending the  $\pi$ -conjugated length of the end groups may provide a new solution for the trade-off of  $V_{oc}$  and  $J_{sc}$  by achieving a red-shifted absorption while minimizing the adverse impact on the LUMO level and thus the  $V_{oc}$ , which has been used much for the design of many small-molecule A-D-A type donors.<sup>32,33</sup> In addition, the introduction of a large  $\pi$ -conjugated moiety onto the end of small molecules would benefit the intermolecular end-to-end  $\pi$ - $\pi$  interaction and molecular packing, leading to enhanced charge separation and transport and thus improving FF.<sup>34</sup> With these, we believe that not only it is urgent and important to design some new NF small-molecule acceptors with extended end conjugation units and study the impact of the end groups overall but also such design might provide molecules with better performance.

Very recently, we reported an A-D-A type small-molecule acceptor 2,9-bis(2-methylene(3(1,1-dicyanomethylene)-indanone))7,12-dihydro-4,4,7,7,12,12-hexaoctyl-4*H*-cyclopenta[2'',1'':5,6;3'':4'':5',6']diindeno[1,2-*b*:1',2'-*b'*]dithiophene (named as FDICTF, Figure 1a) and a PCE of 10.06% with a

Scheme 1. Synthetic Scheme of FDNCTF



high  $V_{oc}$  of 0.94 V for its OSC devices.<sup>35</sup> While we thought the  $V_{oc}$  was high, it seems that there is large potential for the improvement of the  $J_{sc}$  and FF. From the discussion above, we thought that extending the end-group conjugation might be able to manage the trade-off of  $J_{sc}$  and  $V_{oc}$  and achieve the goal of improving the  $J_{sc}$  while maintaining its high  $V_{oc}$ . This is based on the assumption that, different from the approaches of introducing a strong electronegative group on the end,<sup>24,31</sup> the extended end conjugation length/size might not only minimize the impact on the LUMO and thus  $V_{oc}$  but also enhance the light absorption and molecular packing and thus make the  $J_{sc}$  and FF improved simultaneously due to both the appropriately increased D/A interfacial interaction for better exciton separation and the more ordered packing.<sup>34</sup> On the basis of these thoughts, we extended the benzene unit of the previously widely used end group INCN and replaced the benzene unit with a naphthalene unit and synthesized a new active end-group moiety, NINCN (2-(2-oxo-2,3-dihydro-1H-cyclopenta[*b*]naphthalen-1-ylidene)malononitrile). Using NINCN as the end group, a new small-molecule FDNCTF, (2,9-bis(2-methylene-3(1,1-dicyanomethylene)benz[*f*]indanone)-7,12-dihydro-4,4,7,7,12,12-hexaoctyl-4H-cyclopenta[2',1'':5,6;3',4'':5',6']dihydro[1,2-*b*:1',2'-*b'*]dithiophene (Figure 1a), was synthesized. Indeed, the LUMO energy level was little changed compared with the previous molecule FDICTF when INCN was at the end. Importantly, as designed, at solid state, a much red-shifted optical absorption than that of the previous INIC based molecule FDICTF was achieved. This is due to the better molecular ordering than that of FDICTF at solid state arising from the stronger intermolecular interactions between the end groups. In the OSC devices with the same donor material (PBDB-T), due to the appropriately increased D/A interfacial interaction, the charge separation efficiency improved significantly as evidenced by the transient absorption (TA) spectra and other analysis. Thus, the OSCs based on PBDB-T:FDNCTF demonstrated a significantly improved PCE of 11.2% with maintained  $V_{oc}$  and improved  $J_{sc}$  and FF, compared with the corresponding OSCs with FDICTF as the acceptor. These results indicate using extended conjugation end groups might provide another important strategy to design higher performance NF acceptors.

## RESULTS AND DISCUSSION

**Synthesis and Thermal Properties.** The synthetic route of FDNCTF is shown in Scheme 1, and the detailed procedures of it are provided in the Supporting Information (SI). The central unit and its dialdehyde compound FDTCHO have been prepared as before.<sup>36</sup> The Compound 2 (NINCN) was

obtained by Knoevenagel condensation of Compound 1 with malononitrile.<sup>37</sup> The targeted compound FDNCTF was prepared by the Knoevenagel condensation of NINCN and the dialdehyde compound FDTCHO<sup>35</sup> in a 62% yield. The solubility of FDNCTF is quite good in common organic solvents, e.g., chloroform, chlorobenzene, and *ortho*-dichlorobenzene. Thermogravimetric analysis (TGA, Figure S3a) indicates its high thermal stability with the decomposition temperature ( $T_d$ ) of 383 °C with 5% weight loss.

**DFT Calculation.** While the density functional theory (DFT) at the B3LYP/6-31G(d,p) level is probably oversimplified, as it is widely adopted in literatures and consumes less computing power, it was used to investigate the possible influence of the extended end groups on the geometry properties of A-D-A small molecules. If we recall the major steps of the photovoltaic process, including the generation of an exciton by photon absorption, exciton migration/diffusion to the donor:acceptor interface, the charge separation of the exciton at the interface, and the free charge transportation to the electrodes, clearly, the interfacial interaction between the donor and the acceptor plays a critical role for the efficient charge separation of the exciton generated by light absorption. Thus, such interaction, mainly depending on the LUMO orbitals of the donor and acceptor after photo-caused excitation and generation of an exciton (the donor's electron is excited to its LUMO from its HOMO), proper interaction between such two LUMO orbitals could favor an efficient charge separation to generate free charges of electron and hole. Also, such interaction should be not too weak or too strong. Generally, the factors affecting the molecular orbital interaction include the orbital's symmetry, energy difference, overlap, and spatial distance. For our case, with the new end group having a larger and planar conjugation system and considering the general over bulky and rigid core structure of these NF molecules, it is expected that such an expanded end-group structure would enhance the frontier orbital interaction between the donor-acceptor at the interface; thus, a more favorable charge separation process would be achieved to improve the overall photovoltaic performance. With these, we have analyzed the calculated HOMO electron density and LUMO spatial distribution of FDNCTF and FDICTF to understand the effect of the larger end group on the HOMO and LUMO. While the quantitative results may not be accurate, the calculated HOMO electron density and LUMO spatial distribution of FDNCTF and FDICTF in Figure 2a indicate that the new molecule FDNCTF has more LUMO spatial distribution extended to the end. The isosurface of charge density difference of LUMO/HOMO between FDNCTF and

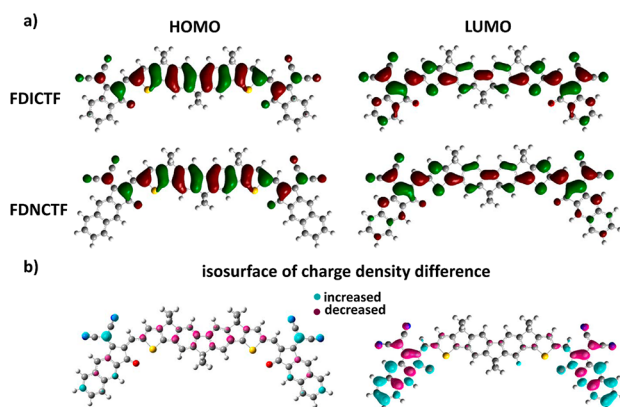


**Figure 2.** (a) Theoretical density distribution for the frontier molecular orbitals of FDNCTF and FDICTF. (b) The isosurface of charge density difference of LUMO (HOMO) between FDNCTF and FDICTF.

FDICTF in Figure 2b offers a clear comparison between these two molecules. As can be seen, the difference between the HOMOs of these two molecules is much smaller than that of their LUMOs. These results indicate that the extended end group significantly changes the LUMO spatial distribution, and makes the spatial distribution in LUMO move down to the end of the molecule. Such a LUMO spatial density in the new molecule would favor an increased D/A interfacial interaction, and if appropriately, thus a more efficient charge separation can be expected.<sup>10,14</sup> Regarding the little change of HOMO distribution, it is intuitive to understand since the HOMO is mainly decided by the central electron-rich group which remains the same for these two molecules.<sup>30,34</sup>

The exciton binding energy in OSC is decided by  $E_q = e^2 / (4\pi\epsilon_0\epsilon_r r_0)$ , where  $e$  is the elementary charge,  $\epsilon_0$  is the permittivity of vacuum,  $\epsilon_r$  is the dielectric constant of the material, and  $r_0$  is the electron and hole separation distance.<sup>38,39</sup> As the  $r_0$  for FDNCTF is naturally larger than that of FDICTF, the  $E_q$  of FDNCTF should be smaller since the dielectric constants of FDICTF and FDNCTF are about the same ( $\sim 2.6$ ) from the measurement (Figure S6). This should also make the exciton of FDNCTF exhibit better charge separation than that of FDICTF, favoring a higher FF and  $J_{sc}$ .

Meanwhile, in order to further investigate the molecular interaction between donor and acceptor in the active layer, the binding energies ( $\Delta G$ ) of both systems with the well-known donor PBDB-T were calculated (Figure S2).<sup>40–42</sup> The binding energy of PBDB-T:FDNCTF is  $-374.0$  kcal/mol, more than that ( $-345.7$  kcal/mol) of PBDB-T:FDICTF (see the SI for details). This indicates an appropriately stronger interaction between PBDB-T with FDNCTF; thus, a more optimized interaction between the donor PBDB-T and acceptor FDNCTF and higher charge separation efficiency would be expected.

### Absorption Spectra and Electrochemical Properties.

As shown in Figure 1d, in chloroform solution, FDNCTF exhibits strong and broad absorption in the region of 550–760 nm with a maximum extinction coefficient of  $3.2 \times 10^5 \text{ M}^{-1} \text{ cm}^{-1}$  at 697 nm, which is higher than that of FDICTF ( $2.7 \times 10^5 \text{ M}^{-1} \text{ cm}^{-1}$  at 665 nm). In thin film (Figure 1e), both FDNCTF and FDICTF exhibit red shifts and broader absorption than their corresponding solution spectra with the maximum absorption peak at 714 nm for FDNCTF and 689 nm for FDICTF. The red-shifted absorption of FDNCTF is consistent with the increased effective  $\pi$ -conjugation.<sup>43</sup> The improved light absorption of FDNCTF should contribute more current than FDICTF. The electronic energy levels of FDNCTF were measured by electrochemical cyclic voltammetry (CV) in dichloromethane (Figure S4). The experimental LUMO energy level of FDNCTF was estimated from the CV to be  $-3.73$  eV, 0.02 eV lower than that of FDICTF. The HOMO energy level ( $-5.43$  eV) of FDNCTF is slightly upshifted compared with that ( $-5.41$  eV) of FDICTF, consistent with the theoretical calculated HOMO/LUMO results of FDICTF ( $-5.56/-3.30$  eV) and FDNCTF ( $-5.52/-3.32$  eV). As expected, FDNCTF as an acceptor exhibits only a slightly lower LUMO energy level, thus minimizing the impact on  $V_{oc}$  of the corresponding OSC devices. The above absorption and energy level data are summarized in Table 1.

**Photovoltaic Properties.** With better absorption and likely better charge separation, it is expected that FDNCTF should have a better photovoltaic performance when the same donor polymer material PBDB-T (Figure 1b) is used. Thus, the OPV devices of this new electron acceptor were fabricated and evaluated with a conventional device configuration of ITO/PEDOT:PSS/PBDB-T:FDNCTF/PDINO/Al, where PDINO is an efficient cathode interlayer developed by Li et al.<sup>44</sup> The detailed device optimization processes are described in the Tables S2–S5, including different donor/acceptor weight ratios, different processing solvents, and solvent additives. The FDNCTF optimized performance was obtained by utilizing chlorobenzene as the processing solvent with donor/acceptor weight ratio 1:0.8 and the active-layer thickness of  $\sim 120$  nm.

The optimized current density–voltage ( $J$ – $V$ ) curve of the device based on PBDB-T:FDNCTF is shown in Figure 3a, and the corresponding photovoltaic parameters are listed in Table 2. Meanwhile, the optimized  $J$ – $V$  and photovoltaic parameters of the PBDB-T:FDICTF device are also provided for comparison.<sup>35</sup> As shown in Table 2, the optimized OSC devices based on PBDB-T:FDNCTF exhibited a high PCE of 11.2% with a  $V_{oc}$  of 0.93 V, a  $J_{sc}$  of  $16.5 \text{ mA cm}^{-2}$ , and an FF of 72.7%. Compared with the FDICTF-based device, the FDNCTF-based device exhibited almost the same  $V_{oc}$  but enhanced  $J_{sc}$ , consistent with the little changed LUMO level and red-shifted and stronger absorption of FDNCTF. Note the FF was improved significantly too. Meanwhile, the FDNCTF-

**Table 1. Optical and Electrochemical Data of FDNCTF and FDICTF**

compd.	$\lambda_{\text{max}}^{\text{sol}}$ (nm)	$\epsilon_{\text{max}}$ ( $\text{M}^{-1} \text{ cm}^{-1}$ )	$\lambda_{\text{max}}^{\text{film}}$ (nm) <sup>a</sup>	$\lambda_{\text{edge}}^{\text{film}}$ (nm) <sup>b</sup>	$E_g^{\text{opt}}$ (eV) <sup>c</sup>	HOMO (eV) <sup>d</sup>	LUMO (eV) <sup>d</sup>	$E_g^{\text{cv}}$ (eV) <sup>e</sup>
FDICTF	665	$2.7 \times 10^5$	689	760	1.63	–5.43	–3.71	1.72
FDNCTF	697	$3.2 \times 10^5$	714	774	1.60	–5.42	–3.73	1.69

<sup>a</sup>Molecular films on quartz plate cast from chloroform solution. <sup>b</sup>Absorption edge of the molecular films:  $E_g^{\text{opt}} = 1240/\lambda_{\text{edge}}$ . <sup>c</sup>Optical band gap was obtained from the onset wavelength of the film. <sup>d</sup>Energy levels evaluated by CV. <sup>e</sup>Electrochemical band gap obtained from  $E_{\text{LUMO}} - E_{\text{HOMO}}$ .

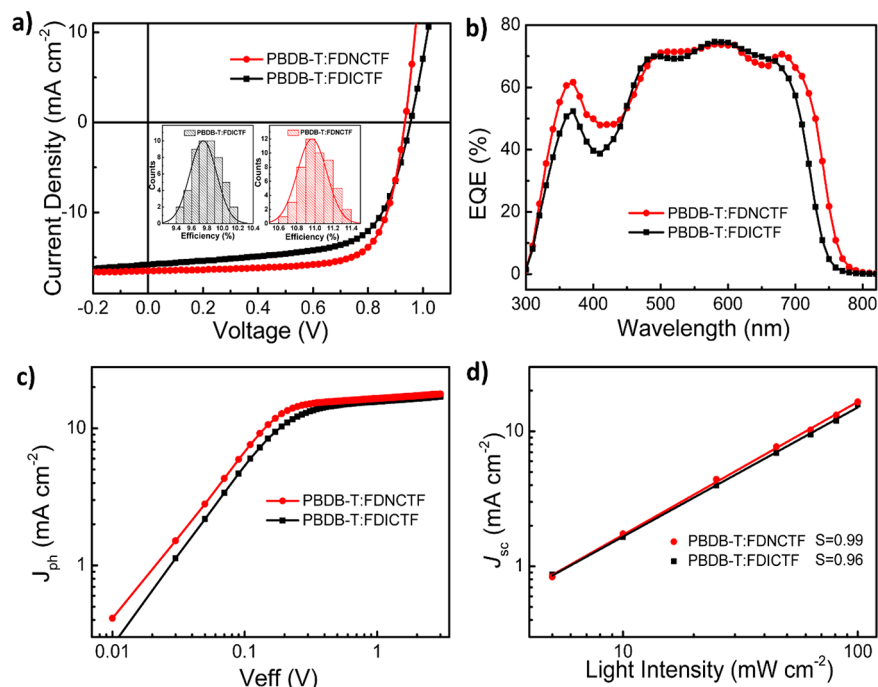


**Figure 3.** (a) Current density–voltage ( $J$ – $V$ ) curves for the devices based on FDICTF and FDNCTF at optimized conditions under the illumination of AM 1.5G ( $100 \text{ mW cm}^{-2}$ ); the inset shows the histograms of the PCE counts for 50 devices. (b) EQE curves for the FDICTF and FDNCTF-based OSC devices. (c)  $J_{\text{ph}}$  versus  $V_{\text{eff}}$  of the optimized devices. (d) Light intensity ( $P$ ) dependence of  $J_{\text{sc}}$ .

**Table 2. Optimized Photovoltaic Parameters of the Devices Based on PBDB-T:FDICTF and PBDB-T:FDNCTF under the Illumination of AM 1.5G ( $100 \text{ mW cm}^{-2}$ )**

acceptor	$V_{\text{oc}}$ (V)	$J_{\text{sc}}$ ( $\text{mA cm}^{-2}$ )	FF (%)	$\text{PCE}_{\text{max}}$ (%)	$\text{PCE}^{\text{b}}$ (%)
FDICTF <sup>a</sup>	$0.94 \pm 0.01$	$15.8 \pm 0.2$	$66.0 \pm 1.0$	10.0	$9.7 \pm 0.2$
FDNCTF	$0.93 \pm 0.01$	$16.3 \pm 0.2$	$72.5 \pm 0.8$	11.2	$10.9 \pm 0.4$

<sup>a</sup>Refer to ref 35. <sup>b</sup>The average PCE value was calculated from 50 devices.

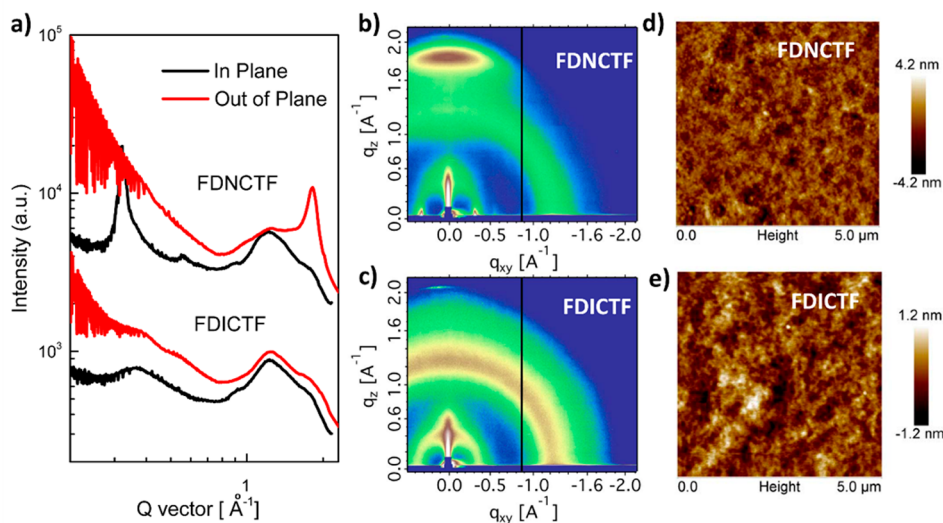


**Figure 4.** (a) The in-plane and out-of-plane line cuts of the GIXD patterns for the FDNCTF and FDICTF. 2D-GIXD patterns for pure films of (b) FDNCTF and (c) FDICTF. AFM height images of (d) FDNCTF and (e) FDICTF films.

based device exhibited decreased energy loss ( $E_{\text{loss}} = E_{\text{g}}^{\text{opt}} - eV_{\text{oc}}$ ) of 0.67 eV comparing with that (0.69 eV) of the FDICTF-based device. The external quantum efficiency (EQE) curve of FDNCTF-based device (Figure 3b) shows stronger and wider photoresponse than that of the FDICTF-based

device, which could be attributed to the stronger and red-shifted absorption of FDNCTF.

To further understand the reasons behind the improved FF of the FDNCTF-based devices, the exciton dissociation, charge collection, and charge recombination were investigated by

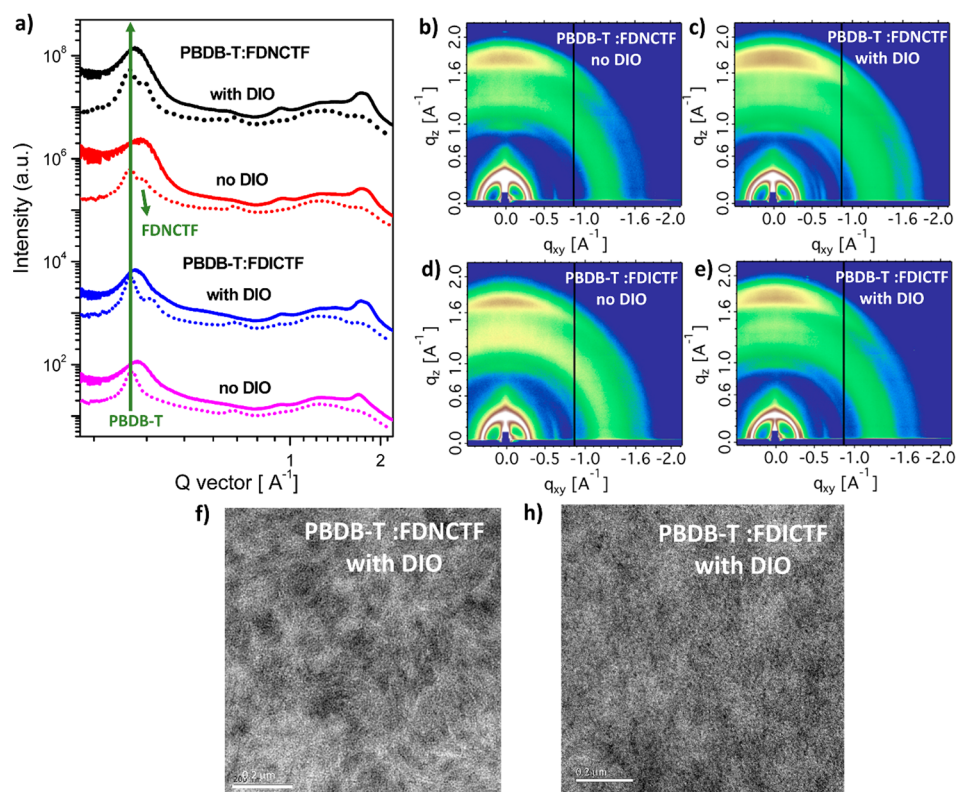


**Figure 5.** (a) The out-of-plane (solid line) and in-plane (dotted line) line-cut profiles of 2D-GIXD patterns. The 2D-GIXD patterns of PBDB-T:FDNCTF blend films (b) without DIO and (c) with DIO; PBDB-T:FDICTF blend films (d) without DIO and (e) with DIO. TEM images of (f) PBDB-T:FDNCTF with DIO and (h) PBDB-T:FDICTF blend films with DIO.

measuring the photocurrent density ( $J_{ph}$ ) versus effective voltage ( $V_{eff}$ ) and the dependence of the  $J_{sc}$  on light intensity.<sup>45</sup> As can be seen from Figure 3c,  $J_{ph}$  values for both devices are saturated ( $J_{sat}$ ) at  $\sim 2$  V, suggesting that charge recombination in both devices is minimized at higher voltage due to the high internal electric field. The  $J_{ph}/J_{sat}$  ratio is up to 93% for the FDNCTF-based devices under short-circuit conditions, compared with 91% for the FDICTF-based devices. Furthermore, these ratios are 80% and 74% for FDNCTF- and FDICTF-based devices, respectively, at the maximal power output conditions. These results indicate that the FDNCTF-based device possesses more efficient exciton dissociation and charge collection relative to those of the FDICTF-based devices, reflecting our initial design. The light-intensity ( $P$ ) dependence of  $J_{sc}$  was also measured to study the charge recombination kinetics.<sup>46</sup> As shown in Figure 3d, the power-law exponents of the equation  $J_{sc} \propto P^\alpha$  for the FDNCTF- and FDICTF-based devices are 0.99 and 0.96, respectively, indicating less bimolecular recombination occurred in the FDNCTF-based device, supporting its improved FF and  $J_{sc}$ .<sup>45,46</sup> In addition, the enhanced fluorescence quenching efficiency (96%) of FDNCTF over that of FDICTF (94%) obtained by the photoluminescence (PL) spectra (Figure S7) indicated a higher exciton dissociation in the PBDB-T:FDNCTF blend. With all of these together, thus a better photovoltaic performance would be expected of FDNCTF-based OSCs than that of FDICTF.

**Morphology Characterization.** To understand why the end-group modulation causes an obvious difference in the photovoltaic performance, the molecular ordering in acceptor thin films was studied using two-dimensional grazing-incidence X-ray diffraction (2D-GIXD). As shown in Figure 4a,c,

FDICTF shows a quite low intensity diffraction peak at around  $0.38 \text{ \AA}^{-1}$  and a strong diffraction halo at around  $1.3 \text{ \AA}^{-1}$ ; thus, it is highly amorphous in neat film.<sup>35</sup> When a larger size of end groups is introduced, the packing of FDNCTF makes a fundamental change. A quite strong (100) lamellar diffraction peak is seen at  $0.32 \text{ \AA}^{-1}$  with an interlamellar distance of  $19.5 \text{ \AA}$  in the in-plane direction; a sharp  $\pi$ - $\pi$  stacking (010) diffraction peak is seen at  $1.82 \text{ \AA}^{-1}$  in the out-of-plane direction with a  $d$ -spacing of  $3.4 \text{ \AA}$  (Figure 4c). Thus, the minor structural change if proper could lead to a completely new molecular ordering, turning an amorphous solid into a highly ordered thin film. The NINCN end group is surely successful in inducing structure order, which can be extended to other material systems. Highly ordered thin film leads to a rough surface. As shown in Figure 4d,e, a larger surface roughness root-mean-square (RMS) of FDNCTF (0.90 nm) is seen over that of FDICTF (0.33 nm). In properties, the electron mobility of FDNCTF ( $2.83 \times 10^{-4} \text{ cm}^2 \text{ V}^{-1} \text{ s}^{-1}$ ) is an order of magnitude larger than that of FDICTF ( $3.79 \times 10^{-5} \text{ cm}^2 \text{ V}^{-1} \text{ s}^{-1}$ ) in a single carrier space-charge-limited current (SCLC) measurement, correlating well with structure details in thin film.

The solid-state packing of molecules in BHJ blends was characterized by 2D-GIXD (Figure 5a–e), transmission electron microscopy (TEM, Figure 5f), and resonant soft X-ray scattering (RSOXS, Figure S10). As shown in Figure 5a,b, the GIXD diffraction of PBDB-T:FDICTF blends without DIO was dominated by the polymer diffraction signals with a (100) peak at  $0.29 \text{ \AA}^{-1}$  and a  $\pi$ - $\pi$  stacking (010) peak at  $1.69 \text{ \AA}^{-1}$ , and there is no clear peak from the acceptor FDICTF. However, PBDB-T:FDNCTF blends processed without DIO showed some differences by comparing Figure 5a,b with Figure

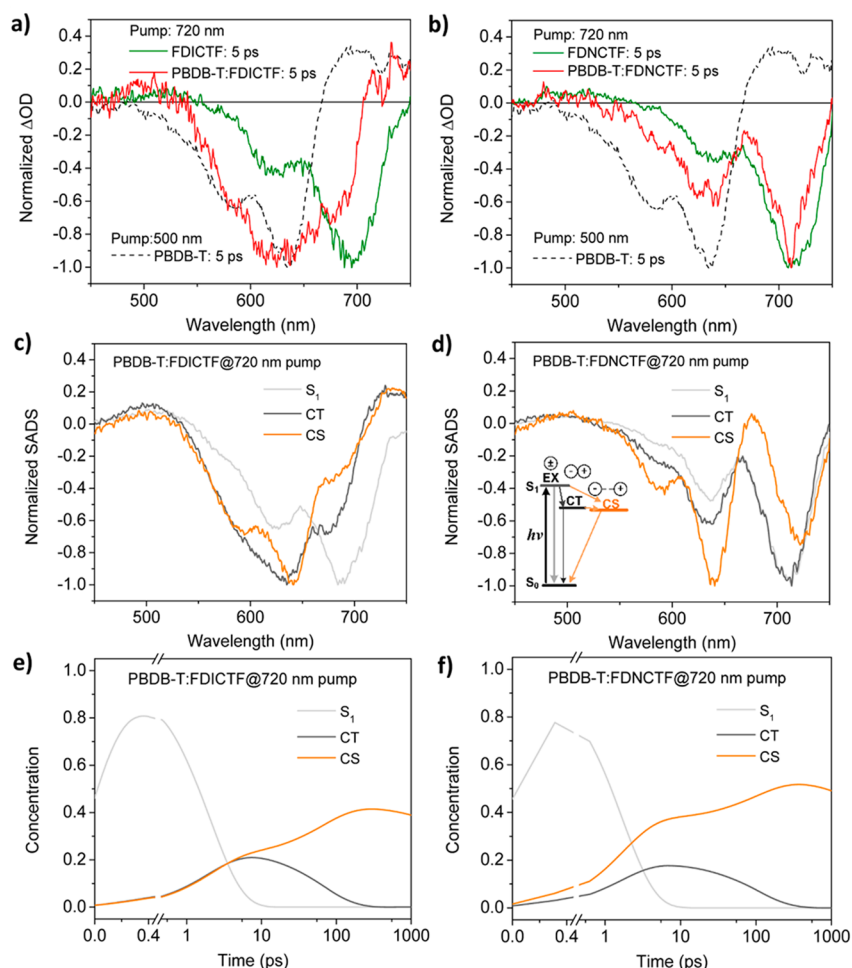


**Figure 6.** (a, b) Differential absorption spectra as a function of probe wavelength with pumping at 500 nm for neat PBDB-T film (black dashed line), at 720 nm for neat FDICTF/FDNCTF (olive solid line), and blends of PBDB-T and FDICTF/FDNCTF films (red solid line) at 5 ps time delay. For better comparison, all spectra shown are normalized to their GSB peaks. (c, d) Target analysis of the normalized transient absorption spectra of PBDB-T:FDICTF (c) and PBDB-T:FDNCTF (d) blend films at 720 nm excitation, which was obtained using the target model shown in the inset. (e, f) Concentrations of the individual species as a function of time.

Sa,d: (1) there is clearly a new peak at  $0.32 \text{ \AA}^{-1}$  from the new acceptor FDNCTF, close to the original polymer (100) peak; and (2) the original (010) peak at  $1.69 \text{ \AA}^{-1}$  has been broadened due to the new acceptor FDNCTF. Thus, the introduced extended end groups could significantly improve the morphology of BHJ blends, with results corresponding well with the device characteristics, owing to the better crystallinity nature of FDNCTF that breaking away from the intimate mixtures with polymer donor.

When a tiny amount of solvent additive was used, the low boiling nature of additive molecules could effectively plasticize the blended thin films, making the glass transition much lower than that of conventional mixtures, and the quicker kinetics of small molecules in self-assembling made pronounced molecular crystals in both cases, which directed better morphologies and thus device performances. As seen from PBDB-T:FDNCTF blends processed with DIO (Figure Sa,c), FDNCTF showed obvious crystallization peaks, which, by fitting, gave a CCL of 20.0 nm (polymer showed a CCL of 22.5 nm.) from in-plane diffraction profiles. While PBDB-T:FDICTF processed with DIO exhibited a rather similar diffraction pattern as shown in Figure Sa,e with that (Figure Sa,c) of PBDB-T:FDNCTF with DIO, quantitatively it gave a CCL of 16.2 nm for FDICTF

(polymer showed a CCL of 24.5 nm.). The original fitting results are provided in Figure S9 with the fitting details and data accuracy. Thus, better crystallization of FDNCTF was observed in its BHJ blends, which should help to improve device performances as shown in previous discussions. However, the global morphology is more complicated than just the crystalline network; the phase separation and material aggregation also played an important role. As seen from TEM characterizations (Figure 5f), PBDB-T:FDNCTF blends processed with additive showed a fibril network structure as well as dark area material agglomerations, but the PBDB-T:FDICTF thin film was smoother under the same electron microscopy resolution and, though a larger in-plane (100) polymer CCL was seen, the fibril network structure was less obvious (Figure 5h). These features were due to the better mixing of PBDB-T and FDICTF, where, as in PBDB-T:FDNCTF blends, the FDNCTF better crystallization led to stronger FDNCTF aggregated domains that defines a multilength scaled morphology (fibril network in small length scale and material aggregation in large length scale). Such a structure was quite well resolved with further help of RSoXS where a length scale of phase separation at around 160 nm was seen for PBDB-T:FDNCTF and the scattering intensity was much stronger

comparing to PBDB-T:FDICTF blends (Figure S10). These morphological features correspond well with their SCLC mobility characterizations, which show the higher hole and electron mobilities of  $1.77 \times 10^{-4}$  and  $1.00 \times 10^{-4} \text{ cm}^2 \text{ V}^{-1} \text{ s}^{-1}$  of PBDB-T:FDNCTF than those of PBDB-T:FDICTF ( $3.37 \times 10^{-5}$  and  $2.40 \times 10^{-5} \text{ cm}^2 \text{ V}^{-1} \text{ s}^{-1}$ ) measured by the SCLC method (Figure S5) and are consistent with the microstructure analysis and accounted for the improved FF in devices.

**Charge Separation Dynamics.** To understand the mechanism for higher performance (meaning higher  $J_{sc}$  and FF) of this end-extended new acceptor, a series of studies were carried out for the decay dynamics of the exciton in the devices. As it is well-known that, different from fullerene acceptors, for NF electron acceptors, the current contribution due to the acceptor absorption is also playing an important role.<sup>47,48</sup> That is, there are two channels for the exciton generation in the NF-based OSCs, including the conventional channel, exciton generated by the donor absorption of photons and another one by the acceptor absorption, and both types of exciton migrate to the D/A interface to achieve charge separation. Thus, both electron transfer (ET) from donor to acceptor and hole transfer (HT) from acceptor to donor are important for the overall charge separation. To investigate both the electron and hole generation processes at the donor-acceptor interfaces, broad-band femtosecond transient absorption (TA) measurements were performed at different pumping wavelengths for selectively exciting the PBDB-T donor (at 500 nm) or acceptors (FDICTF and FDNCTF) (at 720 nm).<sup>47,49</sup> The TA spectra of PBDB-T:FDICTF and PBDB-T:FDNCTF blend films using a 500 nm pump to just excite donor PBDB-T for investigating the ET process is shown in Figure S11. Target analysis results (species-associated difference spectra, SADS, and concentrations) are exhibited in Figure S11c–f. The normalized SADS shows a new feature for the charge-separated (CS) state at 690 nm in PBDB-T:FDICTF blend (Figure S11c) and 720 nm in PBDB-T:FDNCTF film (Figure S11d), respectively. The new feature was ascribed to the ground-state bleaching (GSB) of FDICTF or FDNCTF, indicating that efficient electron transfer (ET) from donor to acceptor occurs in both two blend films. Corresponding fitted exponential decay time constants and amplitudes by the target model are all listed in Table S1, and PBDB-T:FDNCTF blend film shows a slightly faster ET process, compared with that for PBDB-T:FDICTF.

We further investigated and compared the exciton dissociation and hole transfer (HT) processes in the two blend films in detail, since the difference of the acceptors should make the major difference. Figure 6a,b shows the differential absorption spectra for five films: neat PBDB-T, neat FDICTF, neat FDNCTF, and blends of PBDB-T:FDICTF and PBDB-T:FDNCTF. In order to simplify the discussion, FDNCTF is used as an example to demonstrate exciton dissociation and charge (hole) transfer from these TA spectra. The negative features (Figure 6b) resulted from the GSB as excitons are created in neat PBDB-T (with maxima at 630 and 580 nm) and neat FDNCTF (with maxima at 715 and 640 nm) films. The positive broad signals are the excited-state absorption (ESA) of promptly photoinduced exciton (EX) or charge transfer (CT) in these neat films. The normalized TA spectrum for blended PBDB-T:FDNCTF film at 5 ps with pumping at 720 nm shows, in addition to the GSB of neat FDNCTF, a new feature at 635 nm with intensity much higher than that of neat FDNCTF at the same time delay. This evident feature at 635

nm (though much overlap with the GSB of FDNCTF) is clearly ascribed to the ground-state bleaching of PBDB-T because of the similar band shape of ground-state absorption, suggesting hole transfer from FDNCTF to the donor. To extract the exciton decay dynamics from overlapping TA spectra, target analysis was employed for global fitting to obtain SADS (Figure 6d) and concentrations (Figure 6f). The charge-separated (CS) state (generated via intermolecular exciton dissociation or charge transfer; see the inset in Figure 6d) was observed in PBDB-T:FDNCTF blended films with weakening Coulombic attraction at interfaces. A new bleach band peaking at 580 nm in the spectral profile of the CS state relative to CT/EX occurs, which matches the GSB character of the donor, suggesting efficient separation of hole–electron pairs. The relative red shift of the bleach band peak (722 nm) of CS to that (715 nm) of CT in Figure 6d is attributed to the Stark effect induced exciton band shift,<sup>50</sup> further verifying the generation of free carriers (holes). At the same pumping wavelength, the HT process is also seen in PBDB-T:FDICTF blend film (Figure 6c) as the formation of the CS state with clear GSB character of PBDB-T (maxima at 630 and 580 nm). As the fitting results show in Table S1, the hole transfer from FDNCTF to PBDB-T is much faster with a time constant of 4.8 ps than that from FDICTF with a time constant of 9.5 ps, implying a more efficient hole transfer in PBDB-T:FDNCTF than that in PBDB-T:FDICTF. Comparing panels (e) and (f) in Figure 6, there is higher concentration of the CS state for PBDB-T:FDNCTF at 1 ns. In addition, the yield of CS (hole) in PBDB-T:FDNCTF blend is estimated to be about ~54%, much higher than that (~43%) of PBDB-T:FDICTF, confirming the fact that better power conversion efficiency was obtained in PBDB-T:FDNCTF blend. With these results, it is clear that both the current generation channels are favored for the new molecule. These dynamic studies strongly support our initial thought that the end-extended conjugation would improve the charge separation and thus yield a better FF and overall performance under the same situation.

## CONCLUSION

In conclusion, a new small-molecule acceptor FDNCTF with an A-D-A structure and incorporating NINCN as the new extended end group was designed and synthesized. FDNCTF exhibited red-shifted optical absorption, little changed LUMO energy level, higher charge carrier mobility, and more ordered molecular packing. Non-fullerene OSCs using FDNCTF as the acceptor and a wide band gap polymer PBDB-T as the donor demonstrated a high PCE of 11.2% with a  $V_{oc}$  of 0.93 V, a  $J_{sc}$  of  $16.5 \text{ mA cm}^{-2}$ , and an FF of 72.7%, which is much higher than the PCE of 10.06% for the corresponding FDICTF-based device. The higher  $J_{sc}$  and nearly maintained  $V_{oc}$  are benefited from the better complementary absorption and suitable LUMO energy level. The significantly improved FF should be ascribed to the higher charge separation efficiency and efficient hole transfer from FDNCTF to PBDB-T, confirmed by the transient absorption study. These should be due to the appropriately enhanced intermolecular interaction between the donor and the acceptor because of the extended conjugation of the end groups. These results indicate that employing larger conjugation end groups to the small-molecule acceptors is an effective way to enhance both the absorption and the molecular interaction of the NF acceptor while keeping the LUMO level. This should offer a good strategy to manage the difficult balance and trade-off of  $J_{sc}$  and  $V_{oc}$  in many cases and achieve

higher  $J_{sc}$  and FF while keeping the  $V_{oc}$  relatively unchanged, simultaneously. A similar strategy might be applied for the donor design.

## ■ ASSOCIATED CONTENT

### Supporting Information

The Supporting Information is available free of charge on the ACS Publications website at DOI: 10.1021/acs.chemmater.7b02811.

Experimental details, characterization data for the new compounds, thermogravimetric analysis, differential scanning calorimetry, cyclic voltammogram, internal quantum efficiency, photoluminescence spectra,  $J$ - $V$  characteristics of SCLC, NMR spectra, mass spectra, and other device data (PDF)

## ■ AUTHOR INFORMATION

### Corresponding Authors

\*E-mail: fengliu82@sjtu.edu.cn (F.L.).

\*E-mail: htzhang@nankai.edu.cn (H.Z.).

\*E-mail: yschen99@nankai.edu.cn (Y.C.).

### ORCID

Xian Wang: 0000-0003-3520-7397

Andong Xia: 0000-0002-2325-3110

Yongsheng Chen: 0000-0003-1448-8177

### Author Contributions

<sup>||</sup>H.F. and N.Q. contributed equally to this work.

### Notes

The authors declare no competing financial interest.

## ■ ACKNOWLEDGMENTS

The authors gratefully acknowledge the financial support from the Ministry of Science and Technology of China (MoST) (2014CB643502 and 2016YFA0200200), NSFC (91433101, 51422304, 51373078, and 91633301).

## ■ REFERENCES

- (1) Yu, G.; Gao, J.; Hummelen, J. C.; Wudl, F.; Heeger, A. J. Polymer photovoltaic cells: enhanced efficiencies via a network of internal donor-acceptor heterojunctions. *Science* **1995**, *270*, 1789–1791.
- (2) He, Z. C.; Zhong, C.; Su, S.; Xu, M.; Wu, H.; Cao, Y. Enhanced power-conversion efficiency in polymer solar cells using an inverted device structure. *Nat. Photonics* **2012**, *6*, 591–595.
- (3) Li, G.; Zhu, R.; Yang, Y. Polymer solar cells. *Nat. Photonics* **2012**, *6*, 153–161.
- (4) Heeger, A. J. 25th Anniversary Article: Bulk Heterojunction Solar Cells: Understanding the Mechanism of Operation. *Adv. Mater.* **2014**, *26*, 10–28.
- (5) Lu, L.; Zheng, T.; Wu, Q.; Schneider, A. M.; Zhao, D.; Yu, L. Recent Advances in Bulk Heterojunction Polymer Solar Cells. *Chem. Rev.* **2015**, *115*, 12666–12731.
- (6) Zhao, W.; Li, S.; Yao, H.; Zhang, S.; Zhang, Y.; Yang, B.; Hou, J. Molecular Optimization Enables over 13% Efficiency in Organic Solar Cells. *J. Am. Chem. Soc.* **2017**, *139*, 7148–7151.
- (7) Clarke, T. M.; Durrant, J. R. Charge Photogeneration in Organic Solar Cells. *Chem. Rev.* **2010**, *110*, 6736–6767.
- (8) Blom, P. W. M.; Mihailetchi, V. D.; Koster, L. J. A.; Markov, D. E. Device Physics of Polymer:Fullerene Bulk Heterojunction Solar Cells. *Adv. Mater.* **2007**, *19*, 1551–1566.
- (9) Hertel, D.; Bassler, H. Photoconduction in amorphous organic solids. *ChemPhysChem* **2008**, *9*, 666–688.
- (10) Street, R. A. Electronic Structure and Properties of Organic Bulk-Heterojunction Interfaces. *Adv. Mater.* **2016**, *28*, 3814–3830.

(11) Osikowicz, W.; de Jong, M. P.; Salaneck, W. R. Formation of the Interfacial Dipole at Organic-Organic Interfaces: C60/Polymer Interfaces. *Adv. Mater.* **2007**, *19*, 4213–4217.

(12) Perez, M. D.; Borek, C.; Forrest, S. R.; Thompson, M. E. Molecular and morphological influences on the open circuit voltages of organic photovoltaic devices. *J. Am. Chem. Soc.* **2009**, *131*, 9281–9286.

(13) Zhao, Y.; Liang, W. Charge transfer in organic molecules for solar cells: theoretical perspective. *Chem. Soc. Rev.* **2012**, *41*, 1075–1087.

(14) Brédas, J.-L.; Norton, J. E.; Cornil, J.; Coropceanu, V. Molecular Understanding of Organic Solar Cells: The Challenges. *Acc. Chem. Res.* **2009**, *42*, 1691–1699.

(15) Scharber, M. C.; Mühlbacher, D.; Koppe, M.; Denk, P.; Waldauf, C.; Heeger, A. J.; Brabec, C. J. Design Rules for Donors in Bulk-Heterojunction Solar Cells—Towards 10% Energy-Conversion Efficiency. *Adv. Mater.* **2006**, *18*, 789–794.

(16) Cheng, Y.-J.; Yang, S.-H.; Hsu, C.-S. Synthesis of Conjugated Polymers for Organic Solar Cell Applications. *Chem. Rev.* **2009**, *109*, 5868–5923.

(17) Zhang, J.; Xie, S.; Zhang, X.; Lu, Z.; Xiao, H.; Li, C.; Li, G.; Xu, X.; Chen, X.; Bo, Z. Hyperbranched polymer as an acceptor for polymer solar cells. *Chem. Commun.* **2017**, *53*, 537–540.

(18) Tang, A.; Zhan, C.; Yao, J.; Zhou, E. Design of Diketopyrrolopyrrole (DPP)-Based Small Molecules for Organic-Solar-Cell Applications. *Adv. Mater.* **2017**, *29*, 1600013.

(19) Lin, Y.; Zhang, Z.-G.; Bai, H.; Wang, J.; Yao, Y.; Li, Y.; Zhu, D.; Zhan, X. High-performance fullerene-free polymer solar cells with 6.31% efficiency. *Energy Environ. Sci.* **2015**, *8*, 610–616.

(20) Meng, D.; Sun, D.; Zhong, C.; Liu, T.; Fan, B.; Huo, L.; Li, Y.; Jiang, W.; Choi, H.; Kim, T.; Kim, J. Y.; Sun, Y.; Wang, Z.; Heeger, A. J. High-Performance Solution-Processed Non-Fullerene Organic Solar Cells Based on Selenophene-Containing Perylene Bisimide Acceptor. *J. Am. Chem. Soc.* **2016**, *138*, 375–380.

(21) Fernández-Lázaro, F.; Zink-Lorre, N.; Sastre-Santos, Á. Perylenediimides as non-fullerene acceptors in bulk-heterojunction solar cells (BHJSCs). *J. Mater. Chem. A* **2016**, *4*, 9336–9346.

(22) Baran, D.; Ashraf, R. S.; Hanifi, D. A.; Abdelsamie, M.; Gasparini, N.; Rohr, J. A.; Holliday, S.; Wadsworth, A.; Lockett, S.; Neophytou, M.; Emmott, C. J.; Nelson, J.; Brabec, C. J.; Amassian, A.; Salleo, A.; Kirchartz, T.; Durrant, J. R.; McCulloch, I. Reducing the efficiency-stability-cost gap of organic photovoltaics with highly efficient and stable small molecule acceptor ternary solar cells. *Nat. Mater.* **2016**, *16*, 363–369.

(23) Lin, Y.; Wang, J.; Zhang, Z. G.; Bai, H.; Li, Y.; Zhu, D.; Zhan, X. An electron acceptor challenging fullerenes for efficient polymer solar cells. *Adv. Mater.* **2015**, *27*, 1170–1174.

(24) Dai, S.; Zhao, F.; Zhang, Q.; Lau, T. K.; Li, T.; Liu, K.; Ling, Q.; Wang, C.; Lu, X.; You, W.; Zhan, X. Fused Nonacyclic Electron Acceptors for Efficient Polymer Solar Cells. *J. Am. Chem. Soc.* **2017**, *139*, 1336–1343.

(25) Zhao, W.; Qian, D.; Zhang, S.; Li, S.; Inganäs, O.; Gao, F.; Hou, J. Fullerene-Free Polymer Solar Cells with over 11% Efficiency and Excellent Thermal Stability. *Adv. Mater.* **2016**, *28*, 4734–4739.

(26) Zhou, J.; Wan, X.; Liu, Y.; Zuo, Y.; Li, Z.; He, G.; Long, G.; Ni, W.; Li, C.; Su, X.; Chen, Y. Small molecules based on benzo[1,2-b:4,5-b']dithiophene unit for high-performance solution-processed organic solar cells. *J. Am. Chem. Soc.* **2012**, *134*, 16345–16351.

(27) Yao, H.; Cui, Y.; Yu, R.; Gao, B.; Zhang, H.; Hou, J. Design, Synthesis, and Photovoltaic Characterization of a Small Molecular Acceptor with an Ultra-Narrow Band Gap. *Angew. Chem., Int. Ed.* **2017**, *56*, 3045–3049.

(28) Kan, B.; Feng, H.; Wan, X.; Liu, F.; Ke, X.; Wang, Y.; Wang, Y.; Zhang, H.; Li, C.; Hou, J.; Chen, Y. Small-Molecule Acceptor Based on the Heptacyclic Benzodi(cyclopentadithiophene) Unit for Highly Efficient Nonfullerene Organic Solar Cells. *J. Am. Chem. Soc.* **2017**, *139*, 4929–4934.

- (29) Liang, N.; Jiang, W.; Hou, J.; Wang, Z. New developments in non-fullerene small molecule acceptors for polymer solar cells. *Mater. Chem. Front.* **2017**, *1*, 1291–1303.
- (30) Liu, F.; Zhou, Z.; Zhang, C.; Vergote, T.; Fan, H.; Liu, F.; Zhu, X. A Thieno[3,4-b]thiophene-Based Non-fullerene Electron Acceptor for High-Performance Bulk-Heterojunction Organic Solar Cells. *J. Am. Chem. Soc.* **2016**, *138*, 15523–15526.
- (31) Li, S.; Ye, L.; Zhao, W.; Zhang, S.; Mukherjee, S.; Ade, H.; Hou, J. Energy-Level Modulation of Small-Molecule Electron Acceptors to Achieve over 12% Efficiency in Polymer Solar Cells. *Adv. Mater.* **2016**, *28*, 9423–9429.
- (32) Duan, R.; Cui, Y.; Zhao, Y.; Li, C.; Chen, L.; Hou, J.; Wagner, M.; Baumgarten, M.; He, C.; Mullen, K. The Importance of End Groups for Solution-Processed Small-Molecule Bulk-Heterojunction Photovoltaic Cells. *ChemSusChem* **2016**, *9*, 973–980.
- (33) Zhang, Q.; Kan, B.; Liu, F.; Long, G.; Wan, X.; Chen, X.; Zuo, Y.; Ni, W.; Zhang, H.; Li, M.; Hu, Z.; Huang, F.; Cao, Y.; Liang, Z.; Zhang, M.; Russell, T. P.; Chen, Y. Small-molecule solar cells with efficiency over 9%. *Nat. Photonics* **2014**, *9*, 35–41.
- (34) Lee, O. P.; Yiu, A. T.; Beaujuge, P. M.; Woo, C. H.; Holcombe, T. W.; Millstone, J. E.; Douglas, J. D.; Chen, M. S.; Frechet, J. M. Efficient small molecule bulk heterojunction solar cells with high fill factors via pyrene-directed molecular self-assembly. *Adv. Mater.* **2011**, *23*, 5359–5363.
- (35) Qiu, N.; Zhang, H.; Wan, X.; Li, C.; Ke, X.; Feng, H.; Kan, B.; Zhang, H.; Zhang, Q.; Lu, Y.; Chen, Y. A New Nonfullerene Electron Acceptor with a Ladder Type Backbone for High-Performance Organic Solar Cells. *Adv. Mater.* **2017**, *29*, 1604964.
- (36) Buckle, D. R.; Morgan, N. J.; Ross, J. W.; Smith, H.; Spicer, B. A. Antiallergic activity of 2-nitroindan-1,3-diones. *J. Med. Chem.* **1973**, *16*, 1334–1339.
- (37) Feng, H.; Li, M.; Ni, W.; Kan, B.; Wang, Y.; Zhang, Y.; Zhang, H.; Wan, X.; Chen, Y. A series of dithienobenzodithiophene based small molecules for highly efficient organic solar cells. *Sci. China: Chem.* **2017**, *60*, 552–560.
- (38) Cho, N.; Schlenker, C. W.; Kesting, K. M.; Koelsch, P.; Yip, H.-L.; Ginger, D. S.; Jen, A. K. Y. High-Dielectric Constant Side-Chain Polymers Show Reduced Non-Geminate Recombination in Heterojunction Solar Cells. *Adv. Energy Mater.* **2014**, *4*, 1301857.
- (39) Frenkel. On the transformation of light into heat in solids. II. *Phys. Rev.* **1931**, *37*, 1276–1294.
- (40) Grimme, S.; Ehrlich, S.; Goerigk, L. Effect of the damping function in dispersion corrected density functional theory. *J. Comput. Chem.* **2011**, *32*, 1456–1465.
- (41) Li, Y.; Pullerits, T.; Zhao, M.; Sun, M. Theoretical Characterization of the PC60BM:PDDTT Model for an Organic Solar Cell. *J. Phys. Chem. C* **2011**, *115*, 21865–21873.
- (42) Simon, S.; Duran, M.; Dannenberg, J. J. How does basis set superposition error change the potential surfaces for hydrogen-bonded dimers? *J. Chem. Phys.* **1996**, *105*, 11024–11031.
- (43) Kobin, B.; Grubert, L.; Blumstengel, S.; Henneberger, F.; Hecht, S. Vacuum-processable ladder-type oligophenylenes for organic-inorganic hybrid structures: synthesis, optical and electrochemical properties upon increasing planarization as well as thin film growth. *J. Mater. Chem.* **2012**, *22*, 4383–4390.
- (44) Yang, Y.; Zhang, Z. G.; Bin, H.; Chen, S.; Gao, L.; Xue, L.; Yang, C.; Li, Y. Side-Chain Isomerization on n-type Organic Semiconductor ITIC Acceptor Make 11.77% High Efficiency Polymer Solar Cells. *J. Am. Chem. Soc.* **2016**, *138*, 15011–15018.
- (45) Blom, P. W. M.; Mihailtchi, V. D.; Koster, L. J. A.; Markov, D. E. Markov, D. E. Device physics of polymer: fullerene bulk heterojunction solar cells. *Adv. Mater.* **2007**, *19*, 1551–1566.
- (46) Proctor, C. M.; Kuik, M.; Nguyen, T.-Q. Charge carrier recombination in organic solar cells. *Prog. Polym. Sci.* **2013**, *38*, 1941–1960.
- (47) Zhong, Y.; Trinh, M. T.; Chen, R.; Wang, W.; Khlyabich, P. P.; Kumar, B.; Xu, Q.; Nam, C. Y.; Sfeir, M. Y.; Black, C.; Steigerwald, M. L.; Loo, Y. L.; Xiao, S.; Ng, F.; Zhu, X. Y.; Nuckolls, C. Efficient organic solar cells with helical perylene diimide electron acceptors. *J. Am. Chem. Soc.* **2014**, *136*, 15215–15221.
- (48) Bin, H.; Gao, L.; Zhang, Z. G.; Yang, Y.; Zhang, Y.; Zhang, C.; Chen, S.; Xue, L.; Yang, C.; Xiao, M.; Li, Y. 11.4% Efficiency non-fullerene polymer solar cells with trialkylsilyl substituted 2D-conjugated polymer as donor. *Nat. Commun.* **2016**, *7*, 13651.
- (49) Zhao, F.; Li, Y.; Wang, Z.; Yang, Y.; Wang, Z.; He, G.; Zhang, J.; Jiang, L.; Wang, T.; Wei, Z.; Ma, W.; Li, B.; Xia, A.; Li, Y.; Wang, C. Combining Energy Transfer and Optimized Morphology for Highly Efficient Ternary Polymer Solar Cells. *Adv. Energy Mater.* **2017**, *7*, 1602552.
- (50) Gélinas, S.; Rao, A.; Kumar, A.; Smith, S. L.; Chin, A. W.; Clark, J.; van der Poll, T. S.; Bazan, G. C.; Friend, R. H. Ultrafast Long-Range Charge Separation in Organic Semiconductor Photovoltaic Diodes. *Science* **2014**, *343*, 512–516.